Materials and Design 33 (2012) 469–475

Contents lists available at ScienceDirect

Materials and Design

journal homepage: www.elsevier.com/locate/matdes

Transient liquid phase diffusion bonding Al-6061 using nano-dispersed Ni coatings

Kavian O. Cooke [a,*], Tahir I. Khan [a], Gossett D. Oliver [b]

[a] Department of Mechanical and Manufacturing, University of Calgary, 2500 University Drive, NW, Calgary, Alberta, Canada T2N 1N4
[b] Department of Mechanical Engineering, University of Technology, Jamaica, 237 Old Hope Road, Kingston 6, Jamaica

ARTICLE INFO

Article history:
Received 14 February 2011
Accepted 26 April 2011
Available online 4 May 2011

Keywords:
A. Metal–matrix composite
D. Diffusion bonding
H. Failure analysis

ABSTRACT

Transient liquid phase diffusion bonding (TLPDB) of Al-6061 containing 15 vol.% alumina particles was carried out at various bonding temperatures. A 5 μm thick electrodeposited Ni-coating containing 18 vol.% nano-size alumina particles was used at the interlayer. Joint formation was attributed to the solid-state diffusion of Ni into the Al-6061 alloy followed by eutectic formation and isothermal solidification at the joint interface. Examination of the joint region using scanning electron microscopy (SEM), wavelength dispersive spectroscopy (WDS) and X-ray diffraction (XRD) showed the formation of intermetallic phases such as Al_3Ni, Al_9FeNi and Ni_3Si within the joint zone. The results indicate that the incorporation of nano-size Al_2O_3 dispersions into the interlayer can be used to improve joint strength.

1. Introduction

Aluminum metal–matrix composites (Al-MMCs) have been of particular interest to the automotive and aerospace industries, due to their high strength-to-weight ratio, formability and corrosion resistance. However, despite the unique properties of these materials, the lack of a reliable joining method has restricted their full potential in engineering applications [1–4]. In this regard, numerous joining techniques have been studied in an attempt to identify a process that can be successfully used to join Al-MMCs. Some of the processes that have been studied include: fusion welding [1,5–7], brazing [8–11], solid-state diffusion bonding [12,13–16] and transient liquid-phase (TLP) bonding [17,18–21]. The major challenges reported in the scientific literature are; undesirable interfacial reactions between the matrix and reinforcement, particulate segregation and low joint strength.

TLP diffusion bonding has been extensively studied for joining particle reinforced Al-MMCs [1,2,22]. The process depends on the formation of a thin continuous layer of liquid at the joint interface through eutectic or peritectic reaction between the interlayer and the base metal. This reaction also has the advantage of been able to remove surface oxides. The liquid film wets the contacting metallic substrates and solidifies isothermally, followed by homogenization of the joint region [18–20]. The advantage of using this process is that reinforcing particles are incorporated into the bond region either by using a particle reinforced filler material [17] or by the melt-back of the substrate metal [24].

Attempts have been made to improve joint strength [3–17], however, despite the many studies that have been performed the major problems affecting the process have still not been successfully resolved. Metal foil interlayers such as Cu, Zn, Ni and Ag [22,17] are often used in the joining process. Unfortunately, the use of metal foils to join particle-reinforced composites can result in the formation of dispersion free zones (DFZ) within the joint region. Recent studies into joining Al-MMCs have focused on the use of soldering or brazing since these techniques avoid the problems associated with significant base metal melting, and offer improved flexibility in component design and production [23,25]. It was reported that Sn-based interlayers reinforced with SiC are capable of improving joint strength of Al-6061 + 25% (Al_2O_3)p by approximately 100% when compared to unreinforced joints formed by ultrasonic assisted soldering [26]. However, the joint formed normally has a strength far lower than that of the parent metal, and this limits the use of components made by this method to less critical applications. Yan et al. [27] developed a SiC particle reinforced Zn-based filler which was used to join SiCp/A356 composite. The results indicated that without ultrasonic vibration, poor joint properties were achieved. The lower joint strengths were attributed to particle agglomeration and void formation within the joint zone. However when ultrasonic vibration was used suitable particle distribution and reduced void formation were achieved. This work, though promising can only be successfully applied during ultrasonic assisted joining.

In this study a thin composite coating reinforced with nano-sized Al_2O_3 particles is used as a method of enhancing the mechanical strength of the TLP bonded joints. A mathematical equation developed for predicting parent metal dissolution of particle

* Corresponding author. Tel.: +1 403 220 5772.
E-mail addresses: kocooke@ucalgary.ca, kavin_cooke@yahoo.com (K.O. Cooke).

0261-3069/$ - see front matter © 2011 Elsevier Ltd. All rights reserved.
doi:10.1016/j.matdes.2011.04.051

reinforced Al-MMCs when using composite coatings is also presented. The effect of bonding temperature on microstructural development across the joint and subsequent effect on shear strength and failure mechanism was investigated.

2. Materials and methods

2.1. Materials

In this study an Al-6061 alloy containing 15 vol.% of alumina (Al_2O_3) particles with an average size of 28 μm is used. The microstructure and composition of the material is shown in Fig 1 and Table 1 respectively.

2.2. Sample preparation and bonding process

The specimens were prepared for bonding by cutting to a dimension of 10 × 10 × 5 mm. A hole was drilled to a depth of 3 mm at 1 mm from the bonding interface. The bonding surfaces were prepared to 800 grit SiC finish and subsequently polished to a 1 μm diamond-suspension and then cleaned in an acetone bath.

Prior to bonding, one piece of each couple was electroplated with a 5 μm thick Ni-coating co-deposited with 500 nm Al_2O_3 particles. The electrodeposition of Ni onto the Al-6061 surfaces was carried out in a 250 ml glass beaker using Watt's nickel bath recipe [28]. The specimens were assembled at room temperature and placed on the lower platen within the induction coil and an ungrounded *k*-type thermocouple inserted into the hole located approximately 1 mm from the joint interface. Once a vacuum of 4×10^{-4} torr (0.053 Pa) was achieved, the assembly was heated to a bonding temperature ranging from 570 °C to 620 °C. The lower temperature limit of 570 °C was selected to be above the Al–Ni–Si eutectic temperature of 565 °C [29]. The upper temperature limit of 620 °C was selected through preliminary investigations, in which bonding was carried out up to a temperature 640 °C. However, specimens bonded above 620 °C experienced extensive plastic deformation, as such these specimens were discarded.

The specimens were brought to the joining temperature at a heating rate of 65 °C/min and then held at that temperature for 10 min. The power was turned off and the specimen was cooled to room temperature in vacuum, once the bonding process was completed. Bonded specimens were sectioned perpendicular to the bond-line by an abrasive saw and mounted in Bakelite. The mounted specimens were prepared according to ASTM standard B 253 [30]. The samples were ground progressively on silicon carbide papers from 240–800 grit, followed by a final polish to 1 μm finish. A mixture containing 2 ml HF, 3 ml HCl, 5 ml HNO_3 and 190 ml H_2O was used as the etchant to reveal the aluminum grain structure.

Table 1
Composition of Al-6061/15 vol.% Al_2O_3 alloy.

Composition wt.%								
Fe	Cu	Mg	Mn	Cr	Ti	Zn	Si	Al
0.03	0.11	1.09	0.05	0.08	0.09	0.15	0.69	Bal

Bonded samples were machined to 8 mm diameter to eliminate edge effects. Bonded specimens of approximately 12 mm length and 8 mm diameter were loaded into a specially prepared apparatus, which is schematically shown in Fig. 2. The grips of this apparatus were pulled in tension by a Tinius–Olsen tensile testing machine at a cross-head speed of 0.5 mm/min in position control mode such that the specimen experienced pure shear stress across the bond interface. The shear strength was calculated by dividing the maximum load by the bond area. For each bonding condition three specimens were tested and the average value used to determine the shear strength (bond strength).

Examination of the joints was performed using a optical microscope and a scanning electron probe microscopy (SEM). Quantitative compositional analyses were carried out using wavelength dispersive spectroscopy (WDS) and X-ray diffraction (XRD). Micro-hardness testing was performed on the cross-section of the joints according to ASTM E92 standard test method for a Vickers

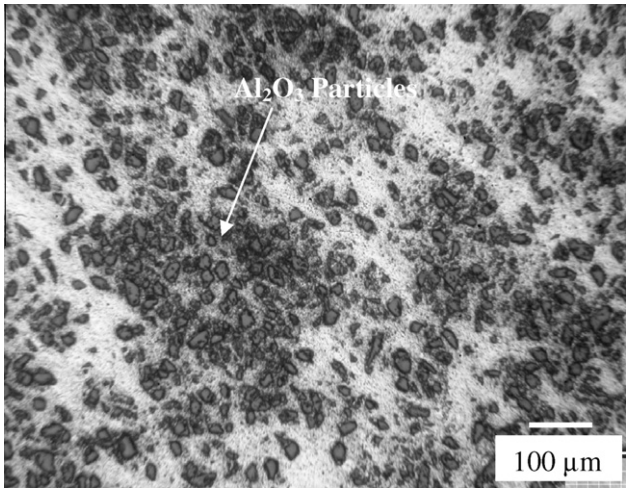

Fig. 1. Microstructure of the Al-6061/15 vol.% Al_2O_3p metal–matrix composite.

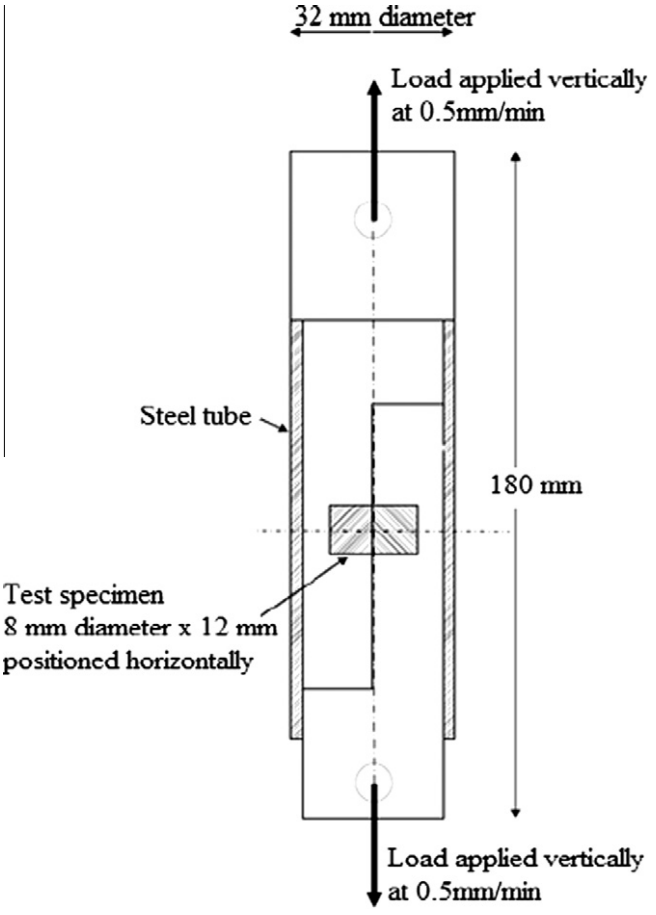

Fig. 2. Schematic of shear test rig.

micro-hardness tester. Indentations were made at 100 μm spacing using a diamond tip indenter to which a 0.2 kg load was applied for 15 s, after which the length of the diagonals were measured and the hardness number recorded form tables.

3. Results and discussion

3.1. Microstructure of the joint

Bonding temperature is one of the most important parameters considered when diffusion bonding aluminum metal–matrix composites. In this study, diffusion bonding was carried out at temperatures ranging from 570 °C to 640 °C. However, samples bonded above 620 °C experienced extensive macroscopic deformation, as such only samples made at bonding temperatures between 570 °C and 620 °C are reported in this paper.

A study of the joint microstructure for a bond made at 570 °C revealed the segregation of Al_2O_3 particles at the bond-line as shown in Fig 3a. When the bonding temperature was increased to 590 °C the width of the segregated zone decreased to approximately 150 μm as shown in Fig. 3b. Further increase in bonding temperature to 600 °C also resulted in a reduction in the width of the segregated zone as shown in Fig 4a. A similar result was obtained when the bonding temperature was increased to 620 °C (see Fig 4b). This observation is consistent with earlier literature which suggests that [21] using a thin interlayer can help to control the degree of segregation at the joint center.

The micrographs shown in Figs 3 and 4 indicate that the width of the segregated zone decreases with increasing bonding temperature. According to earlier research on the solidification characteristic of Al_2O_3 reinforced Al-MMCs, the primary α-phase is very efficient in rejecting the Al_2O_3, and pushing the particles ahead of the solid/liquid interface. In this regard, a critical solid/liquid interface velocity has been reported, above which the Al_2O_3 particles are engulfed by the moving interface and below which they are pushed towards the joint center [31,32].

Table 2 shows the WDS analysis of the joint as a function of bonding temperature. The results indicate that the Ni concentration at the interface decreased from 4.65 wt.% to 0.19 wt.% as the bonding temperature is increased from 570 °C to 620 °C. This was attributed to an increase in the diffusivity of Ni from the interface into the basemetal as the temperature increased. A review of the scientific literature shows that the diffusivity of Ni increased from $D_{570} = 4.69 \times 10^{-13}$ m^2/s to $D_{620} = 1.58 \times 10^{-12}$ m^2/s when the bonding temperature was increased from 570 °C to 620 °C [33,34]. Additionally, the increased diffusivity of Ni into Al resulted in the formation of a large quantity of the eutectic mixture at the grain boundaries as shown in Fig. 5a. The variations of Ni across the joint are also shown in Fig. 5b.

3.2. Modeling parent metal dissolution of Al-MMCs using composite coating

Thin electrodeposited Ni coatings containing nano-dispersions of Al_2O_3were used to produce TLP bonds. Ceramic particles were introduced into the coatings to reinforce the soft metal–matrix and to strengthen the joint region after TLP bonding. The effect of thin coatings on the width of the molten zone can be estimated by applying mass a conservation equation to the molten zone. The mass balance equation for transient liquid phase bonding of particle reinforced aluminum metal–matrix composite using nano-sized particle reinforced composite interlayer can be written as;

$$w_0\rho_C C_B(1-\varepsilon) = (w_{\max} - w_o(1-\varepsilon))(1-v)\rho_A C_{L\alpha} - w_0\rho_A C_{L\alpha}(1-\varepsilon) \quad (1)$$

By rearranging the above equation we obtain:

$$w_{\max} = w_0(1-\varepsilon)\left[\left(\frac{C_B - C_{L\alpha}}{C_{L\alpha} - vC_{L\alpha}}\right)\cdot\frac{\rho_C}{\rho_A} + 1\right] \quad (2)$$

where ρ_C is the density of the composite interlayer, ρ_A is the density of the base-metal, v is the volume fraction of Al_2O_3 reinforcement in the base-metal, ε is the volume fraction of nano-size Al_2O_3 particles in the interlayer, $C_{L\alpha}$ is the vol.% of nickel in the liquid at the bonding temperature, w_0 is the initial width of the interlayer, C_B is the vol.% of nickel in the interlayer and $W_{\max}$ is the maximum width of the liquid zone.

In this study, the values for ρ_C and ρ_A were used as 8.902 g/cm^3, and 2.70 g/cm^3, respectively. The initial concentration C_B of Ni in the interlayer was given a value of 81.4% in the equation. The final concentration of Ni,was taken from the Al–Ni–Si phase diagram [29] to be 8.9 wt.% for a bonding temperature of 620 °C. The volume fraction of Al_2O_3 particles in the interlayer (ε) and the base-metal (v) are 18.4 wt.% and 15 wt.% respectively. Using this information in Eq. (1), $W_{\max}$ was calculated to be 103 μm. When these values are substituted into the equation developed by Tuah-Poku for estimating $W_{\max}$ a maximum dissolution width of 116 μm was calculated [19]. The differences in these values can be attributed to the fact that Tuah-Poku's equation assumes that the entire joint zone forms a liquid. However in this study, at a bonding temperature of 620 °C it is assumed that dissolution of the Al_2O_3 dispersion at the joint interface would not occur. Therefore the volume fraction of reinforcements present in the interface must be subtracted from the eutectic volume formed at the joint region. This provides an accurate estimation of the maximum width of the parent metal dissolved.

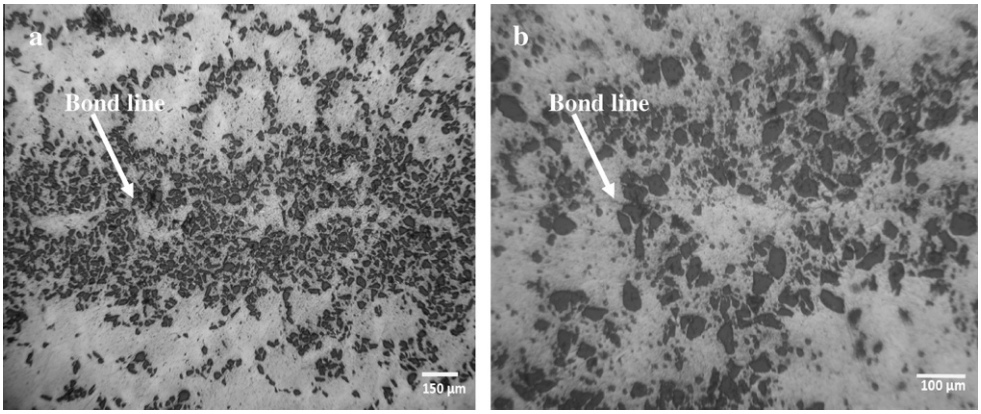

Fig. 3. Light micrographs of the joint microstructures for bonding temperatures of (a) 570 °C and (b) 590 °C.

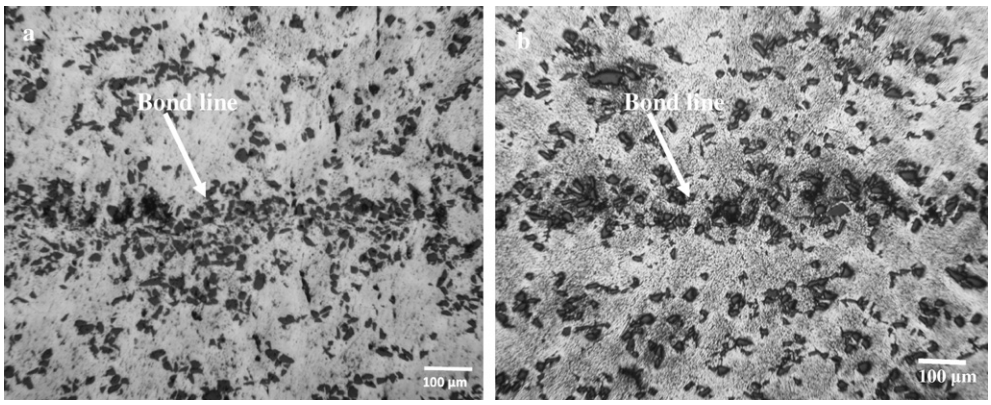

Fig. 4. Light micrographs of the joint microstructure for bonding temperatures of (a) 600 °C and (b) 620 °C.

Table 2
Shows WDS analysis of the joint composition (wt.%) as a function of bonding temperature.

Temperature (°C)	Mg	Ni	Si	Fe	Al
570	2.53	4.65	0.72	0.35	Bal
590	1.73	1.69	0.52	0.28	Bal
600	1.52	0.35	0.41	0.21	Bal
620	0.94	0.19	0.21	0.19	Bal

3.3. Isothermal solidification

Stefanescu [31,32] showed that particle pushing can be assumed to be a steady-state condition under which the interface velocity can be assumed to be equal the rate of isothermal solidification. This rate can be calculated using a model proposed by Sinclair [35,36]. The significance of the constant, ξ, is that, it is an indication of the solidification rate of the system. Increasing ξ results in faster solid/liquid interface motion, and shorter duration of the isothermal solidification stage. Another important consideration in this study is that, ξ is independent of the initial liquid width, thus it is useful to discuss process kinetics in terms of ξ rather than the time required for isothermal solidification when the temperature and initial liquid width are varied. The isothermal solidification rate can be calculated using the following equation

$$\xi = -2(k-1)^{-1}\sqrt{\frac{D}{\pi}}\cdot\frac{\exp\left(\frac{-\xi^2}{4D}\right)}{erfc\left(\frac{\xi}{2\sqrt{D}}\right)} \tag{3}$$

where, k is a partition coefficient given by $\frac{C_{L\alpha}}{C_{\alpha L}}$ and D is the diffusivity.

The final concentration of Ni, $C_{\alpha L}$ was taken from the Al–Ni–Si phase diagram [29] to be 4.9 wt.% for the bonding temperature of

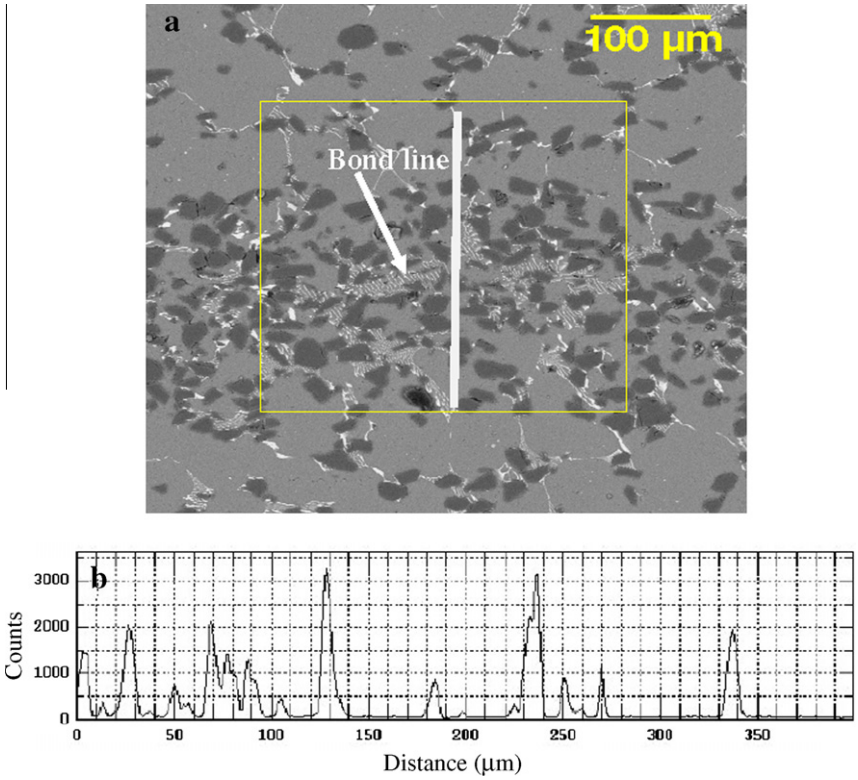

Fig. 5. (a) SEM micrograph of a bond made at 600 °C and (b) WDS line-scan showing the change in concentration of Ni across the interface.

620 °C. The diffusivity of Ni in Al at 620 °C is $D = 1.58 \times 10^{-12}$ m^2/s [35,36]. This increase in diffusivity is reflected in a faster solid/liquid interface rate (ξ) and a shorter isothermal solidification stage [31]. Using these values the predicted interface rate constant $\xi = -0.395$ μm/s was calculated from Eq. (3). This solidification rate is significantly less than the critical interface velocity (16–400 μm/s) required to engulf the particles during solidification [31]. As pointed out by Li et al. [21] segregation tendency is dependent on the relationship between the liquid film width produced at the bonding temperature, particle diameter and interparticle spacing. When the liquid film width is large enough that sufficient particulate material is contained in the melt, particle will be pushed ahead of the solidifying liquid–solid interface resulting in segregation at the bond-line. However if the liquid film width is less than some critical value, segregation should not occur. In Al-MMCs, the segregation of strengthening particles to the joint zone can lead to the formation of particle rich regions, which are susceptible to preferential failure under mechanical loading.

3.4. Micro-hardness measurements

The degree of compositional homogeneity achieved across the joint region was assessed by micro-hardness testing. A uniform value of hardness across the joint would indicate good chemical homogeneity. Micro-hardness profiles are measured as a function of distance from the joint region in both directions. The hardness profiles are shown in Fig. 6.

The profiles show a large variation in the hardness value across the interface at a bonding temperature 570 °C. This is believed to occur as a result of the segregation of Al_2O_3 particles from the base metal into the center of the joint region. When the bonding temperature was increased a significant progressive reduction was seen in the width of the segregated zone present at the joint center. However, the hardness number at the joint center was observed to increase with increasing bonding temperature. The hypothesis is that these differences in hardness at the joint center can be attributed to the presence of nano-sized ceramic particle within the joint region and the precipitation of hard intermetallic compounds. XRD analysis of the polished cross-section of a bonded made at a bonding temperature of 620 °C revealed a high concentration of Al_2O_3 and intermetallics compounds such as: Al_3Ni, Ni_3Si and Al_9FeNi within the joint zone as indicated by Fig 7.

In all profiles shown the highest hardness value was recorded at the joint center and decreased with increasing distance from the joint center. The fluctuation in hardness from the joint zone into the base metal was attributed to the distribution of ceramic particles within the soft metal–matrix phase.

The highest hardness values occurred in joint bonded at 620 °C ranging from 82.3 $HV_{0.2kg}$ to 165 $HV_{0.2kg}$. A more consistent hardness variation is seen across the samples bonded at 590 °C from ranging from 80 $HV_{0.2kg}$ to 110 $HV_{0.2kg}$.

3.5. Shear testing

The shear strength was determined by a single lap shear test. This test method applies localized stress to the joint region therefore it can provide information on the failure mechanisms of the joint region. A comparison of the shear strength as function of bonding temperature is shown in Fig. 8. The strength profile shows that the shear strength increased with increasing bonding temper-

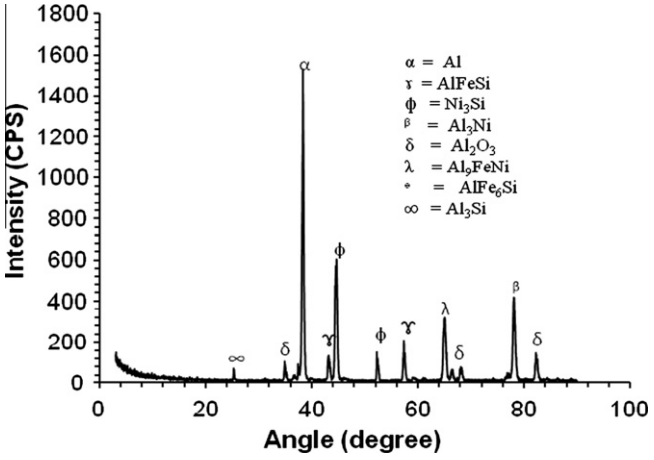

Fig. 7. XRD analysis of the joint cross-section of a bond made at 620 °C.

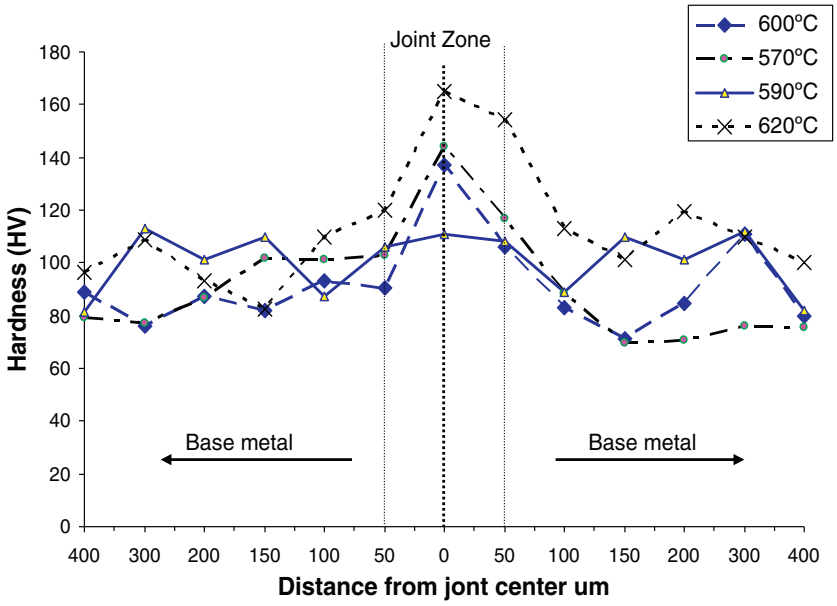

Fig. 6. Effect of temperature on micro-hardness values across the bond interface.

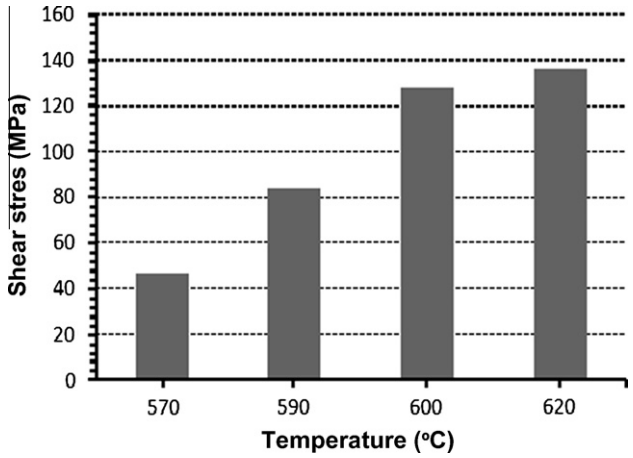

Fig. 8. Effect of bonding temperature on joint shear strengths for joints made using 5 μm thick coatings.

ature, to a maximum value of 138 MPa at 620 °C. The increase in strength was attributed to the presence of nano-sized ceramic particles and precipitation of brittle nickel aluminide phases within the joint region. XRD analysis of the fractured surface of a bonded made at 620 °C is shown in Fig. 11. The results indicate a high concentration of Al_2O_3 and intermetallics compounds such as: Al_3Ni, Ni_3Si and Al_9FeNi at the fractured surface.

In order to compare the effect of bonding temperature on joint failure mechanisms the fractured surfaces were examined using SEM. For a bonding temperature of 570 °C a partially ductile failure was seen (Fig. 9a) with many Al_2O_3 particles visible on the fractured surface. This indicated that at this temperature the matrix-particle (M-P) interface was the weakest point for crack propagation giving the lowest joint strength of (53 MPa). When the bonding temperature was increased to 590 °C a more ductile failure occurred through the base metal adjacent to the bond-line (Fig. 9b). In addition, the number of exposed Al_2O_3 particles at the fractured surface also decreased.

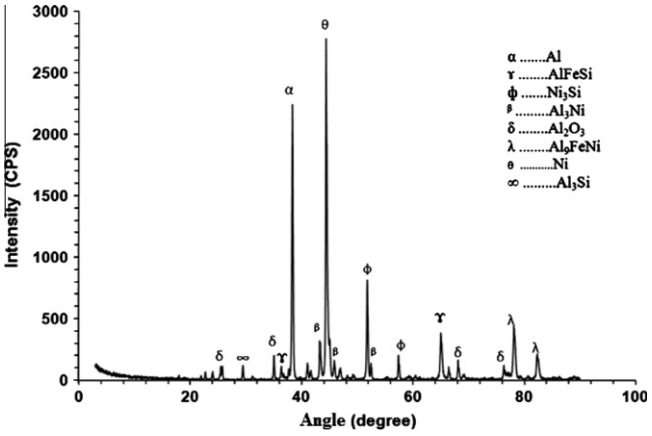

Fig. 11. XRD Analysis of fractured surface of bond made at 620 °C.

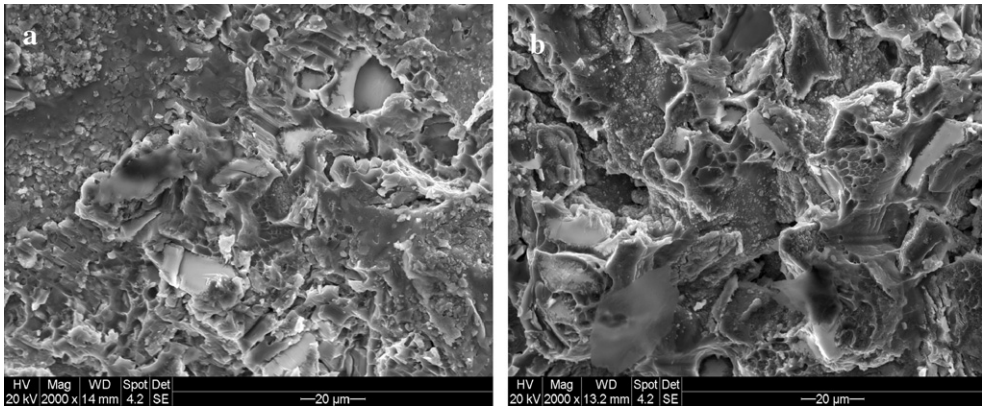

Fig. 9. SEM image of the fractured surfaces of joints made using the 5 μm thick coatings at (a) 570 °C and (b) 590 °C.

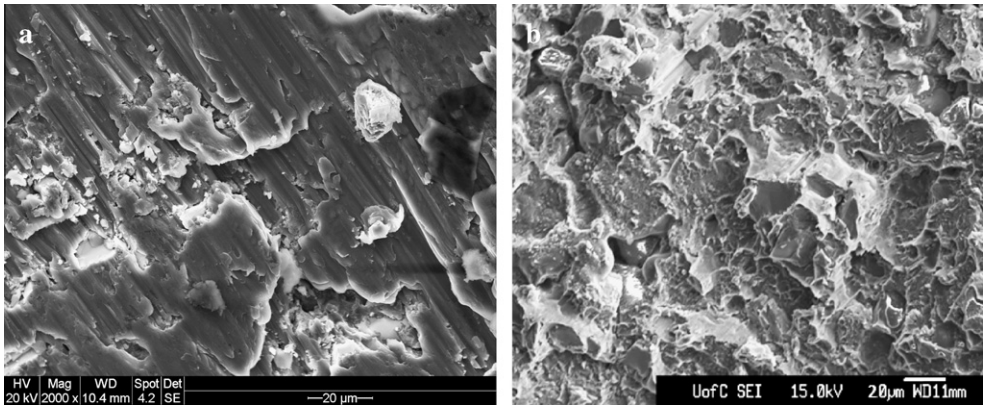

Fig. 10. SEM image of the fractured surfaces of joints made using the 5 μm thick coatings at (a) 600 °C and (b) 620 °C.

A further increase in bonding temperature to 600 °C resulted in a reduction in the concentration of Al_2O_3 particles at the bond interface. Fractographic analysis of the fractured surface showed the presence of dimples along with cleavage facets, indicating mixed mode of failure with crack propagation though the bond-line (Fig. 10a). When that bonding temperature was increased to 620 °C, (Fig. 10b) the fractured surface showed characteristics of a ductile mode of failure, which occurred in the parent metal adjacent to the bond-line. These samples gave the highest joint strength values. The results indicate that the ductility of the joint region increased with increasing bonding temperature. This was attributed to a reduction in the width of the segregated zone with increase in temperature.

4. Conclusion

The results of the study indicates that Al-6061/15%Al_2O_3p aluminum metal–matrix composite can be bonded successfully using transient liquid phase diffusion bonding with the aid of Ni-coating containing a nano-dispersion of Al_2O_3. Joint formation was attributed to a eutectic phase between Al–Ni–Si. The highest joint strength was achieved for bonds made at 620 °C.

The proposed equation for estimating W_{max} during TLP bonding of Al-MMCs using composite interlayer gives a more accurate value for W_{max} than the equation proposed by Tuah-Poku, as it takes into consideration the volume fraction of particulate reinforcement included in both the base metal and the interlayer.

The main factor affecting the joint properties during transient liquid phase diffusion bonding of Al-6061/15%Al2O3p aluminum metal–matrix composite is the distribution of reinforcement particles along the bond interface. It was found that failure occurred directly through particle rich regions.

References

[1] Ellis MBD. Joining of metal–matrix composites: a review. TWI J 1997;6:69–128.
[2] Kumar Pal T. Joining of aluminum metal–matrix composites. J Mater Manuf Processes 2005;20:717–26.
[3] Devletian JH. SiC/Al metal–matrix composite welding by a capacitor discharge process. Weld J 1987;66:33–9.
[4] Wang S, Zhou H, Kang Y. The influence of rare earth elements on microstructures and properties of 6061 aluminum alloy vacuum-brazed joints. J Alloys Compd 2003;352:79–83.
[5] Urena A, Escalera MD, Gil L. Influence of interface reactions on fracture mechanisms in TIG arc-welded aluminum matrix composites. Compos Sci Technol 2000;60:613–22.
[6] García R, López VH, Kennedy AR, Arias G. Welding of Al-359/20%SiCp metal–matrix composites by the novel MIG process with indirect electric arc (IEA). J Mater Sci 2007;42:7794–800.
[7] Yu-cheng L, Wei-jin Y, Xi-zhang C, Fei Z, Xiao-nong C. In-situ weld-alloying plasma arc welding of SiCp/Al MMC. Trans Nonferrous Met Soc China 2007;17:313–7.
[8] Liu L, Tan J, Liu X. Reactive brazing of Al alloy to Mg alloy using zinc-based brazing alloy. Mater Lett 2007;61:2373–7.
[9] Zheng C. Study on brazing technology of aluminium metal–matrix composites with SiC particle reinforcements. Light Alloy Fabr Technol 2004;32(03). translated.
[10] Zhang XP, Quan GF, Wei W. Preliminary investigation on joining performance of SiCp-reinforced aluminum metal–matrix composite by vacuum brazing. Composites Part A 1999;30:823–7.
[11] Weng WP, Chuang TH. Interfacial characteristics for brazing of aluminum matrix composites with Al-12Si filler metals. Metall Mater Trans A 1997;28A:1997–2673.
[12] Feng T, Chen X, Wu L, Lou S. Diffusion welding of SiCp/2014Al composites using Ni as interlayer. J Univ Sci Technol Beijing Miner Metall Mater 2006;13(3):267–71.
[13] Partridge PG, Dunford DV. The role of interlayers in diffusion bonded joints in metal–matrix composites. J Mater Sci 1991;26:2255–8.
[14] Partridge PG, Shepherd M, Dunford DV. Statistical analysis of particulate interface lengths in diffusion bonded joints in a metal–matrix composite. J Mater Sci 1991;26:4953–60.
[15] Zhang XP, Ye L, Mai YW, Quan GF, Wei W. Investigation on diffusion bonding characteristics of SiC particulate reinforced aluminum metal–matrix composites (Al/SiCp-MMC). Compos Part A Appl Sci Manuf 1999;30:1415–21.
[16] Urena A, Gomez de Salazar JM, Escalera MD. Diffusion bonding of an aluminum–copper alloy reinforced with silicon carbide particles (AA2014/Sic/13p) using metallic interlayers. Scr Mater 1996;35:1285–93.
[17] Huang J, Dong Y, Zhang J, Wan Y, Zhou G. Reactive diffusion bonding of SiCp/Al composites by insert powder layers with eutectic composition. J Mater Sci Technol 2005;21(5).
[18] Macdonald WD, Eager TW. Transient liquid phase bonding processes minerals. Met Joining Soc 1992:93–101.
[19] Tuah-Poku I, Dollar M, Massalski TB. A study of the transient liquid phase bonding process applied to a Ag/Cu/Ag sandwich joint. Trans. A 1988;19A:675–86.
[20] Zhou Y, Gale WF, North TH. Modelling of transient liquid phase bonding. Int Mater Rev 1995;40(5):181–96.
[21] Li Z, Zhou Y, North TH. Counteraction of particulate segregation during transient liquid-phase bonding of aluminum-based MMC material. Mater Sci 1995;30:1075–82.
[22] Zhang G, Zhang J, Pei Y, Li S, Chai D. Joining of Al2O3p/Al composites by transient liquid phase (TLP) bonding and a novel process of active-transient liquid phase (A-TLP) bonding. Mater Sci Eng A 2008;488(1–2):146–56.
[23] Zhong XL, Gupta M. High strength lead-free composite solder materials using nano-Al_2O_3 as reinforcement. Adv Eng Mater 2005;7(11).
[24] Shirzadi AA, Wallach ER. New approaches for transient liquid phase diffusion bonding of aluminum based metal–matrix composites. Mater Sci Technol 1997;13:135–42.
[25] Weis S, Hoyer I, Wielage B. Joining of high-strength aluminum-based materials with/tin-based solders. Weld J 2008;86:35–7.
[26] Wielage B, Hoyer I, Weis S. Soldering aluminum matrix composites. Weld J 2007;86:67–70.
[27] Yan Jiuchun, Xu Zhiwu, Shi Lei, Ma Xing, Yang Shiqin. Ultrasonic assisted fabrication of particle reinforced bonds joining aluminum metal–matrix composites. Mater Des 2011;32:343–7.
[28] Dennis JK, Such TE. Nickel and chromium plating. 3rd ed. Woodhead publishing and ASM international; 1993.
[29] Dmitry E, Belov G, Akensov NA, Adrey A. Multicomponent phase diagrams applications for commercial aluminum publisher. Elsevier Science; 2005.
[30] ASTM E3-01 Standard preparation for metallographic examination. ASTM International; 2008.
[31] Stefanescu DM, Juretzko FR, Dhindaw BK, Catalina A, Sen S, Curreri PA. Particle engulfment and pushing by solidifying interfaces: Part II microgravity experiments and theoretical analysis. Metall Mater Trans A 1998;29A:1697–706.
[32] Mukherjee S, Stefanescu DM. Liquid convection effects on the pushing–engulfment transition of insoluble particles by a solidifying interface: Part I analytical calculation of the lift forces. Metall Mater Trans A 2004;35A:613–21.
[33] Askew JR, Wilde JF, Khan TI. Transient liquid phase bonding of 2124 aluminum metal–matrix composite. Mater Sci Technol 1998;14:920–4.
[34] Gale WF, Totemeier TC. Smithells metals reference book. 8th ed. Published by Elsevier; 2004.
[35] Sinclair CW. Modelling transient liquid phase bonding in multi-component systems. J Phase Equilib 1998;20(4).
[36] Sinclair CW, Purdy GR, Morral JE. Transient liquid-phase bonding in two-phase ternary systems. Metall Mater Trans A 2000;31A:1187–92.